Chapter VII

Bio-relevance and hemocompatibility of Eu^{3+}:Gd_2O_3 and Eu^{3+}:$GdVO_4$ nanosystems

Beneficial usage of NPs can be realized only if their potentially harmful and adverse effects are studied in detail with emphasis on interaction in the nano-bio interface test-bed. Important biochemical as well as biophysical mechanisms occurring in the nanoscale hence requires our attention, at large [1, 2]. Reports describe that nanoparticles can be translocated from the lungs into the blood, depending on their size and can thus move to vital organs/tissues [3]. It is noteworthy that in biomedical domain, apart from evaluating the toxicity relevant to size related effects, the material composition of the nanosystem demand detailed and equal emphasis, as different systems may also cause oxidative stress-mediated toxicity at different levels [2, 3].

Intravenous administration of paramagnetic nanoparticles would lead them to be exposed initially to blood and hence NPs can pose various hemotoxic threats *via.* processes such as haemolysis and/or blood coagulation [4]. Shape transformation of red blood cells (RBCs) in addition to reactive oxygen species (ROS) generation due to nanoparticle-erythrocyte interaction is also accompanied by other factors such as activation, aggregation and adhesion of platelets, ultimately leading to membrane rupture [5, 6]. Such loss of erythrocyte membrane integrity or haemolysis envisages haemoglobin release through ruptured cells [4]. Moreover, NPs are known to cause haemolytic effects mediated through several processes *viz.* alterations in their rheological properties, oxidative damage of cell membranes, imbalance of osmotic presence etc. [7].

The ability of RBC, as a model of non-phagocytic cell, to undergo shape deformation and haemolysis after interaction with natural and synthetic compounds is widely used to estimate the cytotoxicity of chemical compounds in general [8-10]. Thorough investigation of change of erythrocytic shapes is a classic problem in the domain of cell biology and over the past three decades, the domain has also fascinated the consideration of physicists [11]. Human RBCs are treated as prototypical cells in order to have an in depth investigation of effects such as shape transformations facilitated by external forces and nanoparticles-cell

membrane interaction via estimating changes in structure and function using high resolution SEM [6, 12]. Morphological transformations of erythrocytes can also be used for evaluating and estimating the hemocompatibility of nanomaterials [4].

Erythrocytes have two leaflets- outer and inner, which constitutes the biconcave shape of the RBCs providing a unique discoid shape, essential for attaining required deformability essential for cell survival following circulation through narrow capillaries [13]. The inner leaflet comprises negatively charged phosphatidylserine which creates a substantial charge difference between the two leaflets [14]. The contents lie enclosed within the leaflets by a network of cytoskeletal and membrane proteins while other cytoplasmic structures are absent *viz.* nucleus, Golgi bodies and endoplasmic reticulum [13, 15]. Furthermore, membrane skeleton (MS), a 2D cross-linked protein cytoskeleton lies inside the plasma membrane [11]. NPs-plasma protein interaction have shown previously to cause adverse physiological changes and biological functions [16]. Hence, evaluation of hemocompatibility, based on plasma-NP interaction is extremely crucial for nanosafety evaluation prior to for effective nanomedicine design in prototype form.

In this chapter, we try to evaluate the haemolytic activity of gadolinium oxide (GNP and 3% EuGNP) as well as vanadate based nanosystem (GdV and 3% EuGdV) against human blood. Furthermore, the effect of NP interaction with the erythrocytic membrane is evaluated using SEM imaging. In addition, an assessment of NP-Plasma interaction is made following determination of plasma recalcification time (PRT) upon treatment with NPs.

7.1.Experimental techniques

7.1.1 Collection of Blood and preparation of Platelet Poor Plasma (PPP)

Fresh human blood was collected voluntarily from a healthy donor (29Yr old without any medication for at least ~72 h prior to collection) and was immediately mixed with anti-coagulant (0.11M tri-sodium citrate) in 9:1 ratio [17]. This was followed by standard centrifugation at ~3000 rpm, ~15 mins (Thermo Scientifc,

USA, Heraeus Multifuge X1R) for separation of the red blood cells (RBC) and platelet poor plasma (PPP), which were collected accordingly in different vials for further usage.

7.1.2. Direct hemolytic activity

RBC pellets obtained were washed thoroughly 3-4 times and then re-suspended in 0.9% (w/v) saline to a final concentration of 10% (v/v). The samples at varying concentrations were incubated (~1 h, 37°C) with 150 µl of 10% RBC to a final volume of 2 µl with 0.9% (v/v) NaCl. This was followed by centrifugation ~5000 rpm, 10 min (Thermo Scientifc, USA, Heraeus Multifuge X1R). Finally, absorbance of supernatant was measured at ~540 nm utilizing a MultiSkanGO, UV-Vis spectrophotometer (Thermo Scientifc, USA).

7.1.3. SEM imaging of erythrocytes

For SEM imaging, RBCs (untreated and treated) were fixed following addition of 2.5% (v/v) glutaraldehyde (for a time duration of 4 h at a temperature of 4°C). PBS washing of fixed cells was followed by drying by performing a series of dehydration using various concentrations of ethanol (50% → 60%, 10 min → 70%, 10 min → 80%, 10 min → 90%, 15 min → 95%, 15min). The dried samples were then cells were then mounted on cover slips. A blood drop was spread along base of the cover slips width using smooth end of spreader to make a proper tail on the slide. The prepared slides were then observed under various magnifications under SEM and images were obtained.

7.1.4. Plasma recalcification time

The plasma recalcification time (PRT) was measured following protocol first reported by Quick *et al*., in which 50 µl of PPP was incubated with appropriate concentration of nanostructures and then 50 µl of 25mM $CaCl_2$ was added to initiate coagulation cascade [18]. To record the clotting occurred, absorbance at 405 nm was checked at 1 min intervals employing a MultiSkanGO, UV-Vis spectrophotometer (Thermo Scientifc, USA)®.

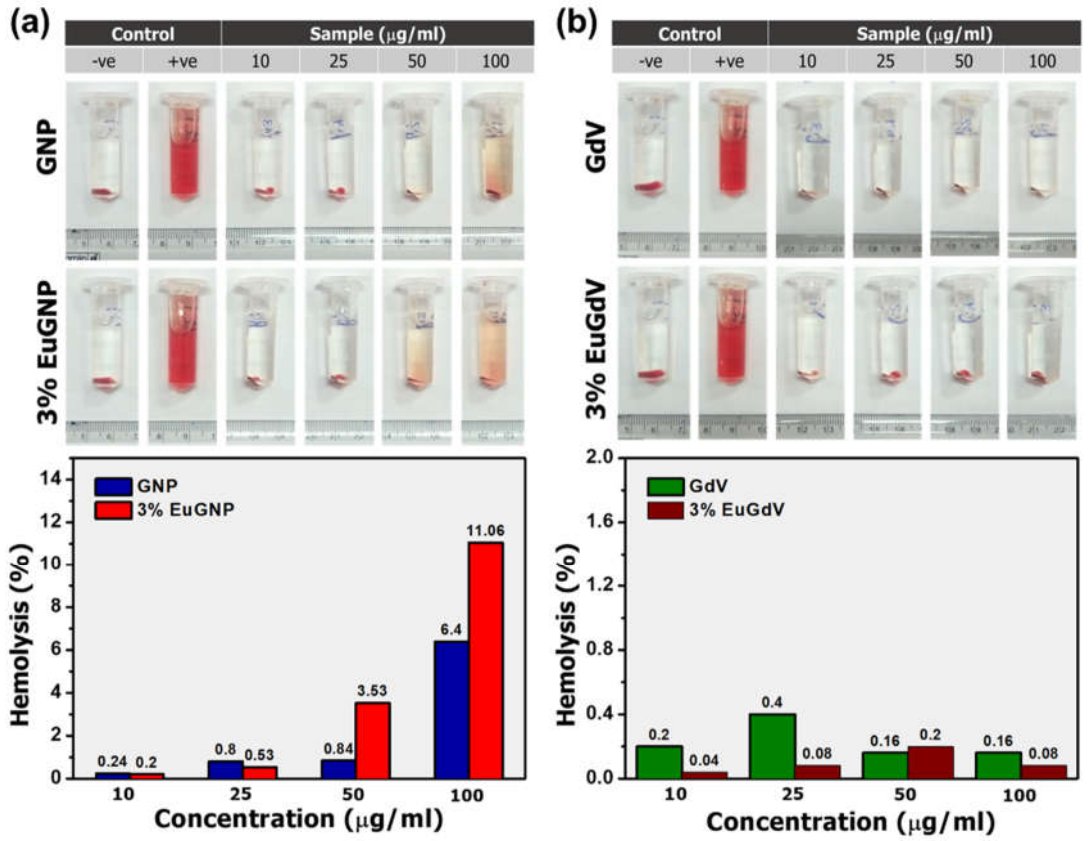

FIGURE 7.1. Hemolytic activity of (a) GNP and 3% EuGNP and (b) GdV and 3% EuGdV.

7.2. Results and Discussion

7.2.1. Hemolytic activity

Nanoparticles are known to interact closely with the membrane to be eventually internalized in the cells thereby causing cell death. Erythrocytes lack internal structure and the interactions with a foreign object are thus revealed following shape transformations which can easily be studied using a microscope under high magnification [12]. Along with change in shape, nanoparticle-erythrocyte interaction also result in reactive oxygen species(ROS) generation, platelet activation, aggregation and adhesion which eventually leads to membrane rupture and thereby lysis [5].

The percent hemolysis of RBCs was calculated using the following expression, which has been adopted from previous reports [19-21]:

$$\% \, hemolysis = \frac{A_{sample} - A_{neg}}{A_{pos} - A_{neg}} \times 100 \qquad (1)$$

In **Eq. 1**, A_{sample}, A_{neg} and A_{pos} are absorbance at 550nm determined for sample, negative control and positive control respectively.

In **FIGURE 7.1**, we observe dose dependent haemolytic activity of GNP and 3% EuGNP. In comparison, 3% EuGNP displayed relatively higher hemolysis up to ~11% at moderate concentration of 100 μg/ml. Concentrations below 100μg/ml can thus be considered as viable to RBCs. Haemolysis refers to damaged erythrocyte membranes and if the haemolysis rate is higher than 5%, the rate is considered significant [4]. Interestingly, toxicity of Gd based compounds and nanosystem could be utilized in the treatment of cancer [8]. Internalization of free Gd^{3+} ions within human immortalized leukemia K562 cells have reportedly induced decrement of their viability *in vitro* [22]. The nanoparticle-cell membrane interactions cause generation of ROS which builds an oxidative stress responsible for breakdown of membrane lipids, along with and DNA breakage and other adversities [2, 23]. Oxidative overload is the main source to cellular damage resulting in alteration of redox state and destruction of the defence-repair systems of the cell [23].

Meanwhile, GdV and EuGdV samples displayed excellent hemocompatibility with minimal or no hemolysis at higher concentrations as well. Lower toxicity can also be related to the fact that at higher concentrations of nanoparticles in a biological medium, agglomeration is prominent resulting in larger aggregates which in general can be responsible for a decrement in hemolytic activity [24].

7.2.2. Time dependent morphological features of nanoparticle treated RBCs

Under no external stress, healthy mammalian RBCs remain disc-shaped (discocytes). In isotonic solutions, erythrocytes are biconcave disc (flattened and bilaterally indented) shaped and carry oxygen in their cytoplasm. While the inner

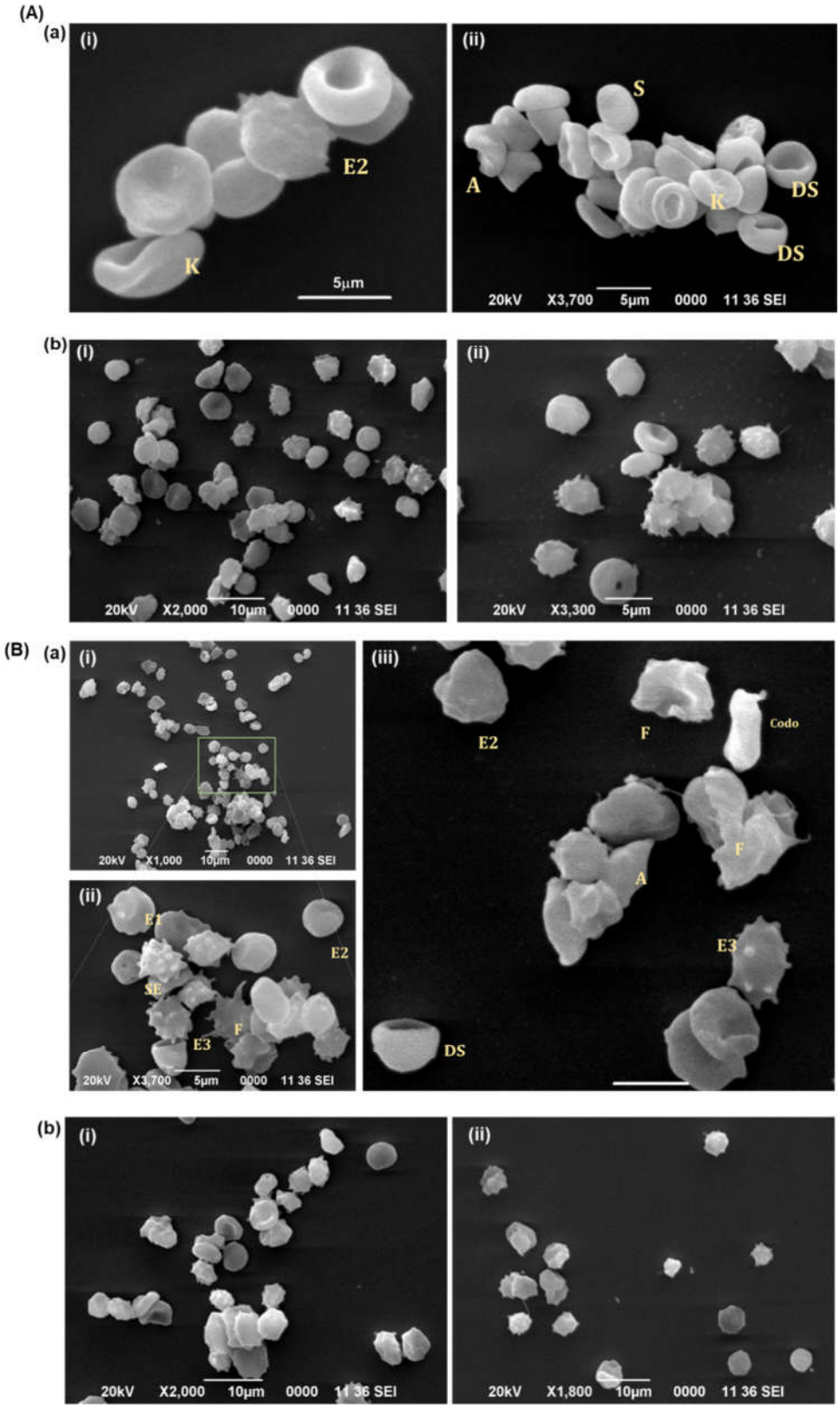

FIGURE 7.2: The SEM images for RBCs (A) untreated (positive control) and (B) hemolysed (negative control) incubated at 37C for (a) 1h and (b) 24h

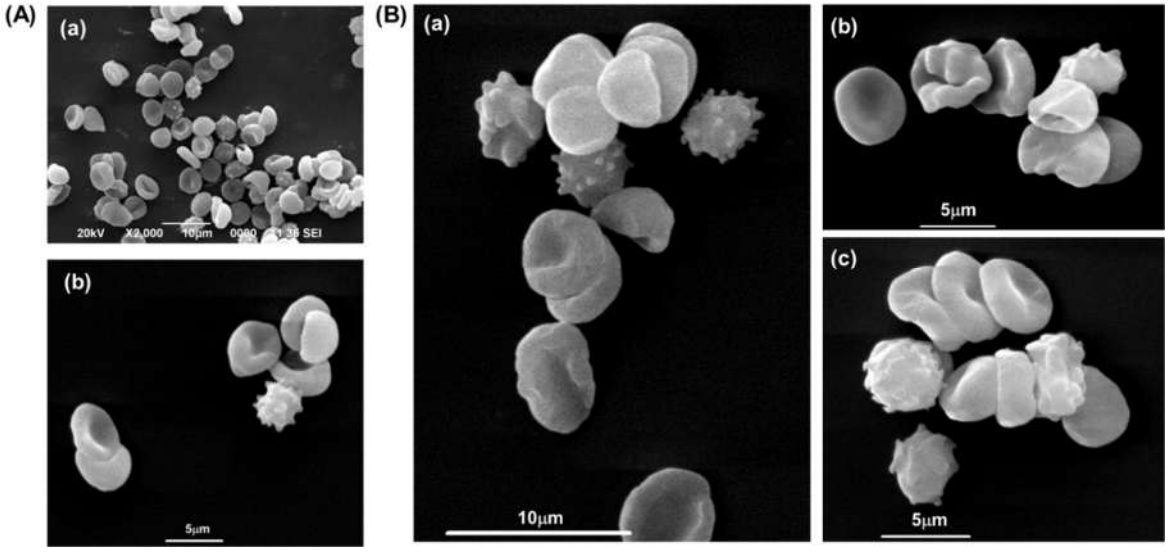

FIGURE 7.3: The SEM images for RBCs treated with 3% EuGNP and incubated for a time duration of (A) 1h and (B) 24h respectively.

phospholipid bilayer with shear resistance contributes to bending resistance and helps to maintain cell surface area needed for easy circulation, it is the outer spectrin network which is principally accountable for the shear elastic properties of the RBC [13]. RBCs maintain its resting biconcave shape by balancing elastic forces within the membrane, along with surface tension, electrical forces on the membrane surface and osmotic/ hydrostatic pressures [25, 26] It is widely accepted that haemolysis is dependent directly upon degree of stretching of the membrane which increases the cell surface area [27, 28]. Spherically shaped cells would be more prone to any deformation with increase in area, and hence the disc shaped feature of erythrocytes is vital [27]. The disc shape thus facilitates microcirculation as well as oxygen carriage [29]. Also external agents are responsible for transformation of erythrocytes into less symmetric shapes such as echinocytes and stomatocytes or even into non-axisymmetric biconcave shapes, in a systematic manner [30, 31]. It is noteworthy that the elastic bending energy is the most dominant feature responsible for maintaining the equilibrium in membrane shape. Meanwhile when fixed for imaging purposes, the shape appears circular corresponding to the indented regions. Any deformations in the cell shape thus defines irregularity in the internal processes essential for proper

cell functioning with their physiological roles being perpetually damaged **[4].** Expansion of outer leaflet (relative to the inner one) offering transformation into convex structures on cell surface known as echinocytic spicules to cover for the area lost [30]. Conversely, concavities or stomatocytic shapes are observed for contraction of inner leaflet. This explanation is known as bilayer-couple hypothesis [31, 32].

FIGURE 7.2 - 7.5 showed the SEM images displaying increased number of irregularly shaped cells upon incubation for a time period of 24 h. The SEM imaging of CTRL0 illustrated healthy control RBC normocytes sized ~6 to 8 µm with normal biconcave discoid shapes of red blood cells and similar shapes were observed even upon 1hr incubation (**FIGURE 7.2**). While upon 12 h of incubation, crenation over a few RBCs appeared. Schistocytes observed in SEM images of CTRLX may have been arisen from the fragmentation of normal erythrocytes involving haemolysis and typically is a consequence of the shearing effect of erythrocytes (**FIGURE 7.3**) [33]. Furthermore, empty and retracted membranes, i.e. erythrocyte-ghosts were observed which are resultant of numerous completely ruptured erythrocytes [12].

Upon treatment with NPs, SEM images demonstrated both aberrant and abnormal morphology of lysed RBCs (**FIGURE 7.4, 7.5**). We observe that along with elliptocytes and microcytes, the number of other cell shapes (such as knizocytes, spherocyte with membrane-bound vesicles, knizodacryocyte, stomatocyte, leptocyte) increases. The cell membranes were found to be disintegrated, deformed and crumbled. Such observation of increasing level of swollen cells is particular for haemolysis [34]. The widely accepted sequence of transformation of erythrocyte shape is as follows: Initial rest discoid shape state of RBC - echinocytic state - intermediate discoid state - final stomatocytic state [30]. Furthermore, upon treatment with nanosystem for a longer duration of the time, the proportion of acanthocytes and elliptocytes was found to be amplified with observance of multiple spicules [15]. Furthermore, various cells displayed

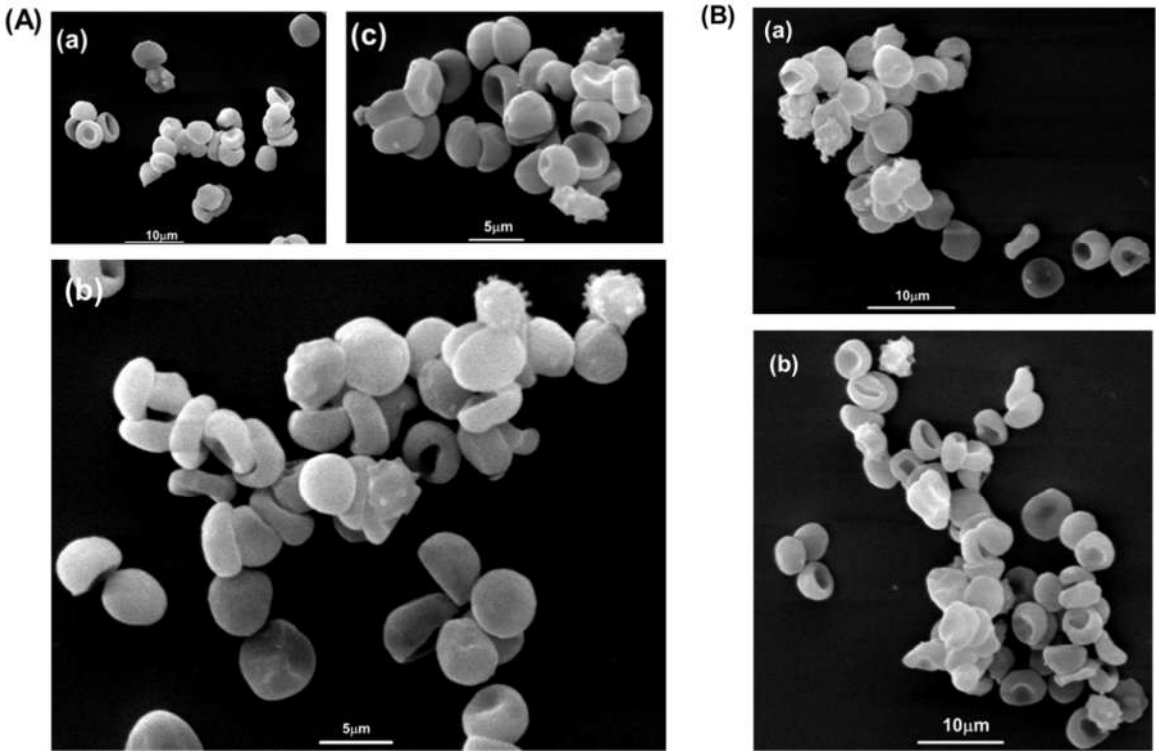

FIGURE 7.4: The SEM images for RBCs treated with 3% EuGdV incubated for (A) 1h and (B) 24h respectively.

destruction of normal discoid shape and cell adhesion was also observed. These morphological abnormalities reflect disruption in the cells' cytoskeleton [15]. The agglomeration of RBCs can be explained citing attractive interaction between membranes induced by nanoparticle-membrane interaction following spatial distribution of charge within the mediating nanoparticles without being strongly bonded to the MS [5, 6]. Moreover, a single individual particle can also enable interaction between two or more MS by empowering a bridging interaction [6]. The descriptive account of percentage of RBCs at various stages of transformation as observed from SEM images is given in **TABLE 1**.

It is known that blood incubated for a prolonged time duration can lead to spectrin oxidation thereby forming lipid vesicles comprising membrane detachment from the cytoskeleton [29]. This in turn leads to loss of membrane structure and compels shape transformation by facilitating necessary cell surface energy essential for normal functioning. Also, oxidative stress affects cytoskeletal

TABLE 1. Percentage of cells of various shape transformation stages calculated using SEM imaging of RBCs.

% of cells	CTRL O		CTRL X		3% EuGNP		3% EuGdV	
	1h	12h	1h	12h	1h	12h	1h	12h
Normal	68.4 ± 2.2	32.7 ± 1.2	3.8 ± 0.3	1.7 ± 0.2	35.9 ± 1.1	22.6 ± 1.1	64.3 ± 2.4	56.5 ± 2.1
Transforming	18.4 ± 0.6	32.7 ± 1.1	7.6 ± 0.1	6.9 ± 0.4	32.8 ± 1.6	35.5 ± 1.2	21.9 ± 0.9	31.5 ± 1.4
Damaged	13.2 ± 1.4	30.9 ± 1.8	18.2 ± 0.8	14.7 ± 0.6	27.5 ± 1.4	28.2 ± 1.1	11.0 ± 0.3	7.5 ± 0.2
Hemolysed	0.0 ±0.0	3.6 ± 2.2	71.2 ± 3.1	78.4 ± 3.6	3.8 ± 0.4	7.3 ± 0.1	3.3 ± 0.2	4.0 ± 0.1

protein adversely such that their ability to interact with spectrin-actin meshwork is compromised and thereby underpins the erythroid membrane [29, 35] . The NP exposure can lead to interruption of phospholipids of the outer membrane and thus alters the outer and inner leaflet surface areas resulting in morphological modifications [30, 36]. The NPs mediation RBC shape deformation is in general related to interaction between NPs-erythrocyte-MS membrane which limits and confines its degree of flexibility of resulting in damage and deformability of erythrocytes [37].

NPs can facilitate formation of complexes upon enhanced interaction with charged glycolipid coat of the erythrocyte membrane [6]. Nanoparticles upon encountering blood cells are coated with proteins that may go through conformational alterations, resulting in exposure to first-hand epitope and altered function [38]. NPs- MS proteins interaction are known to convert erythrocytes them into echinocytes [37, 39]. Deformability, as observed in our case, might as well be a consequence of shearing stress generated upon nanoparticle treatment

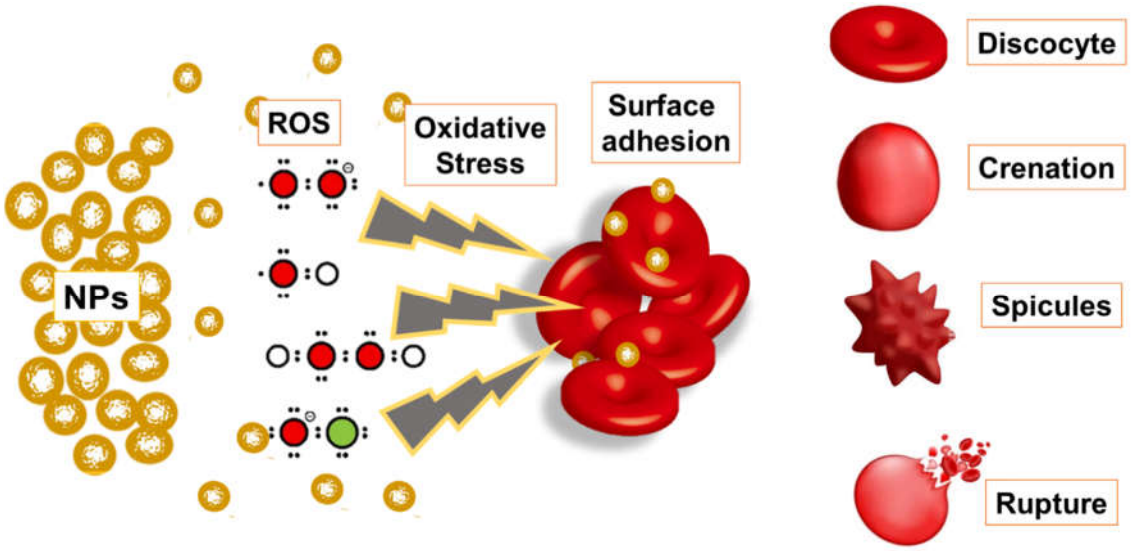

FIGURE 7.5. Schematic illustration of effect of NPs in RBCs shape transformation and consequently lysis.

leading to transformations *viz*. (a) spherical shaped due to hypotonicity (b) discocyte-echinocyte (c) discocyte-stomacyte [35]. In echinocytes, the spicules turn smaller in size as they grow in number to eventually bud off irreversibly. This process forms extracellular vesicles leaving behind a typical spherical body with reduced area/volume (the sphero-echinocyte) [31].

Thus the echinocyte transformation can be demonstrated in four stages- (i) irregularly contouring of the RBC disc (ii) crenation over the flat surface (iii) appearance of spicules over surface and finally transforms into (iv) the sphero-echinocyte cell shape (**FIGURE 7.5**) [35]. Meanwhile, discocyte-stomacyte transformation occurs in two stages and is considered to be a consequence of lowering of pH and/or presence of cations. Furthermore, crenate shape of erythrocytes can be accredited to the manifestation of concentrated haemoglobin within the cellular cytosol [40]. Surface adhesion of NPs on erythrocytic membrane are also considered to play significant role in alterations in morphology [36].

Such alterations are necessary as enhances curvature implies smaller contact surface and hence lower haemolytic cytotoxic potential [41]. Furthermore,

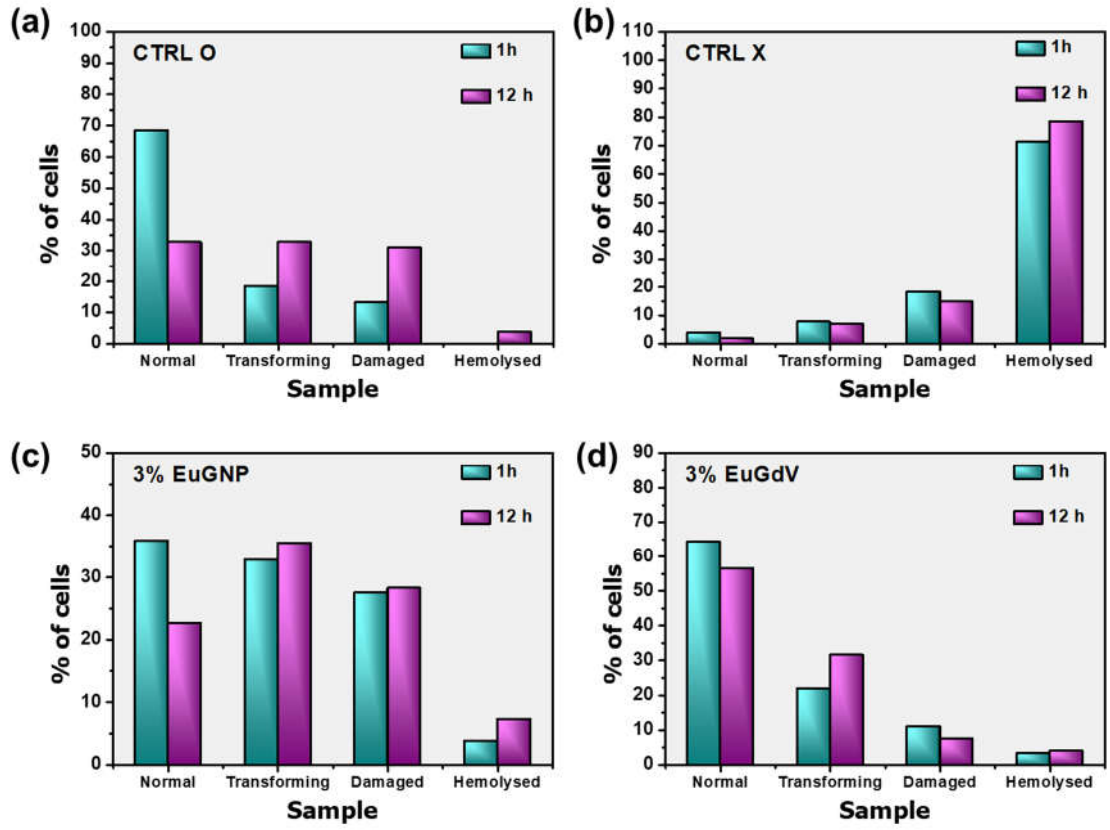

FIGURE 7.6: Comparative plots for the variation in cells of different shapes following different incubation times upon treatment of (a) positive control (b) negative control (c) 3% EuGNP (d) 3% EuGdV.

encapsulation of NPs can also lead to abnormalities in cell shape forming pores (50-200 nm) allowing membrane permeabilization [36, 42]. Also, sulphated proteoglycans molecules (negatively charged) over cell surfaces are extremely crucial for various cellular processes such as proliferation, migration, and motility [43]. These proteoglycans are also responsible for the overall negative membrane charges of the cells. The negatively charged domains predominantly repel negatively charged nanoparticles [43]. Cationic sites available for adsorption of negatively charged particles in the form of clusters via electrostatic interaction can lead to localized neutralization and a subsequently bending of the membrane favouring in turn endocytosis for cellular uptake to occur [43, 44]. This is turn facilitates better cellular uptake of negatively charged NPs as compared to positive counterpart. It is also noteworthy that cationic interaction with the MS of

erythrocytes lead to an increase in the membrane microviscosity compromising its integrity and thereby rupture of cells by aggravated oxidative stress [39, 45]. Under no external factor, the anionic compounds are preferentially bound to the outer half of the lipid bilayer and therefore expand the area of the outer surface relative to the inner surface of the membrane, and cause the cell to crenate; on the other hand, the cationic ones to the inner half cause the cell to form cup shapes [46]. This explains our observation of proportionately greater occurrence of damaged spherocytes and echinocytes as compared to transforming crenated cells in case of cationic Gd_2O_3 nanosystem (zeta potential ~+20-34 mV) as compared to that anionic $GdVO_4$ nanosystem(zeta potential ~ -9-35 mV) (**FIGURE 7.6**) **[47-55].**

Also, effect of oxide nanopowders on the erythrocyte morphology due to production of reactive oxygen species has also been ventured in literature [45, 56]. The ROS formation results in oxidation of free unsaturated fatty acids and their residues. The phospholipids of erythrocyte MS structure thereby upsurges cellular permeability leading to cellular inflammation resulting in a spherical shape as observed [45]. Other factors responsible for echinocytic transformation include increment of intracellular Calcium ion concentration in addition to ATP depletion as a consequence of degradation of endogenous RBC proteins upon nanoparticle treatment [57-59].

7.2.3. Plasma recalcification time

According to the cascade model of coagulation, also referred to as ''enzyme amplifier'' system [60], plasma coagulation process entails a series of chronologically arranged enzymatic reactions executed by coagulation factors activated through two discrete pathways: the cell-mediated tissue factor (TF) pathway and the surface-mediated contact pathway triggered by contacting damaged blood surface [60-62]. Although distinct, both pathways unite to a common pathway causing active thrombin generation and fibrin clot formation, important for blood clotting processes [60]. Autoactivation is the commencing step of the surface-contact activation of Hageman factor into an active enzyme

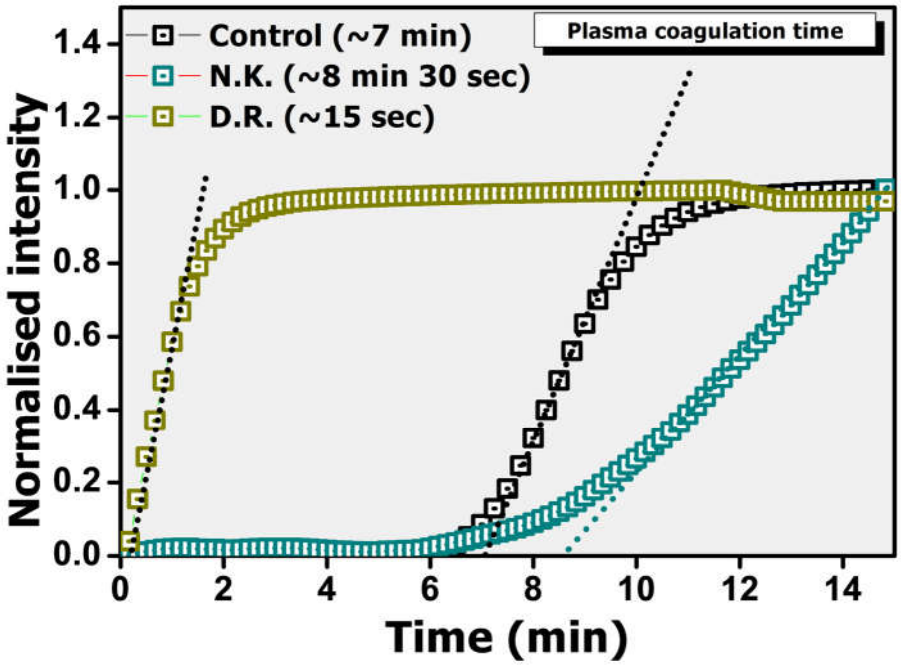

FIGURE 7.7 : Plasma coagulation time for untreated plasma taken at control and under treatment with known anti-coagulant *Naja kaouthia* and pro-coagulant *Daboia russelii* snake venoms

form [61]. Most of such proteolytic reactions take place on anionic phospholipid membrane surfaces from activated platelets which also involve Ca^{2+} as a cofactor [60, 63].

PRT indicates the activation of intrinsic coagulation cascade which is defined by the time required for clot formation enabling us to explore common coagulation pathways [64]. It is note that absorbance as a function of time reveals variation in turbidity due to the presence of fibrins in the clot. The "plateau" in the absorbance profile as shown in **FIGURE 7.7** thereby is symbolic to stable clot [65]. The control plasma exhibited clotting time to begin at ~7 min (**FIGURE 7.7**). The control plasma PRT was compared with PRT upon treatment with snake venoms, a known coagulant- *Daboia russelii* (~15 sec) and anti-coagulant *Naja kaouthia* (~8 min 30 sec).

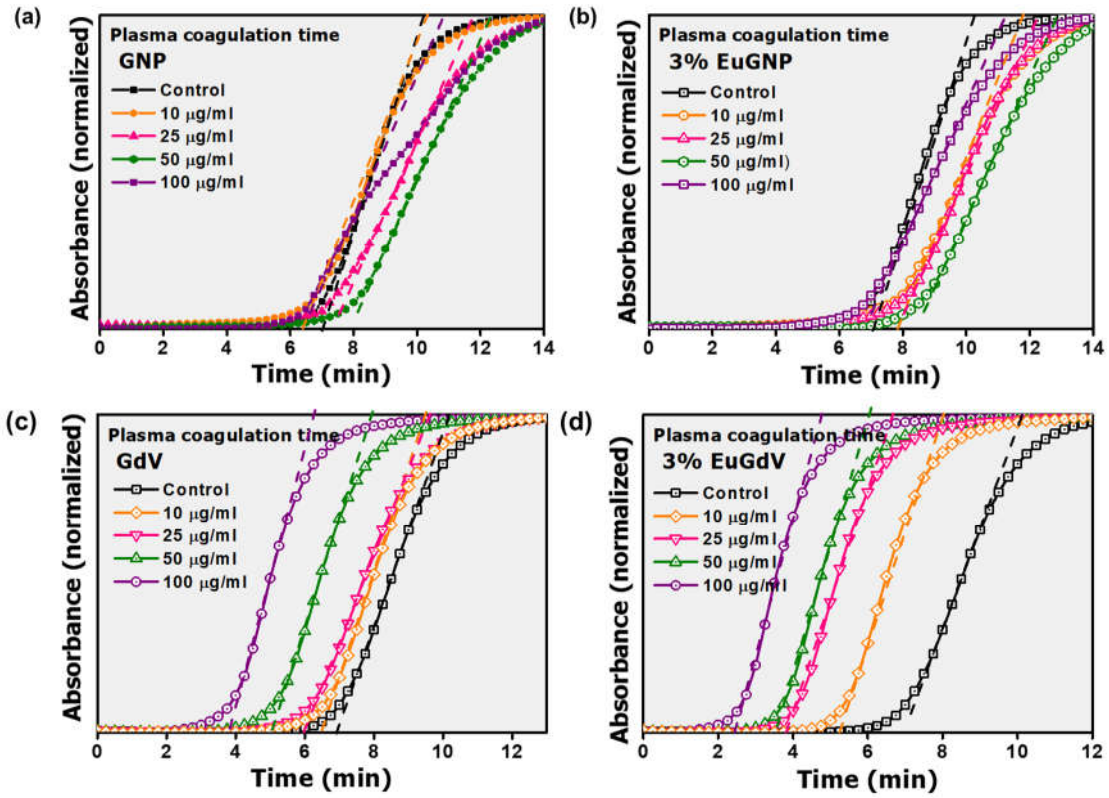

FIGURE 7.8: Plasma recalcification time for various concentrations of (a) GNP (b) 3% EuGNP (c) GdV and (d) 3% EuGdV respectively taken against control and compared with known coagulant Dabia Russeli snake venom and anti-coagulant Naja Kauthia.

The PRT upon treatment with the nanostructures is described in **FIGURE 7.8.** We did not obtain any recognizable alteration in PRT upon GNP and EuGNP. Meanwhile, GdV and EuGdV displayed pro-coagulative activity in a dose dependent manner. The $PRT_{1/2}$ parameter represents concentration of the nanosystem critical to halved as that of the control recalcification clotting time. $PRT_{1/2}$ was determined to be 100 µl and 50 µl for GdV and 3% EuGdV nanosystem as can be seen from **FIGURE 7.9.** Clearly coagulation is more pronounced in case of 3% EuGdV nanosystem.

Protein corona containing coagulation factors can lead to inactivation *i.e.* unavailability of the factor to other components and consequently prolongation in coagulation can be observed. Moreover, it can lead to contact activation of coagulation factors which may result in undesirable coagulation. Increased

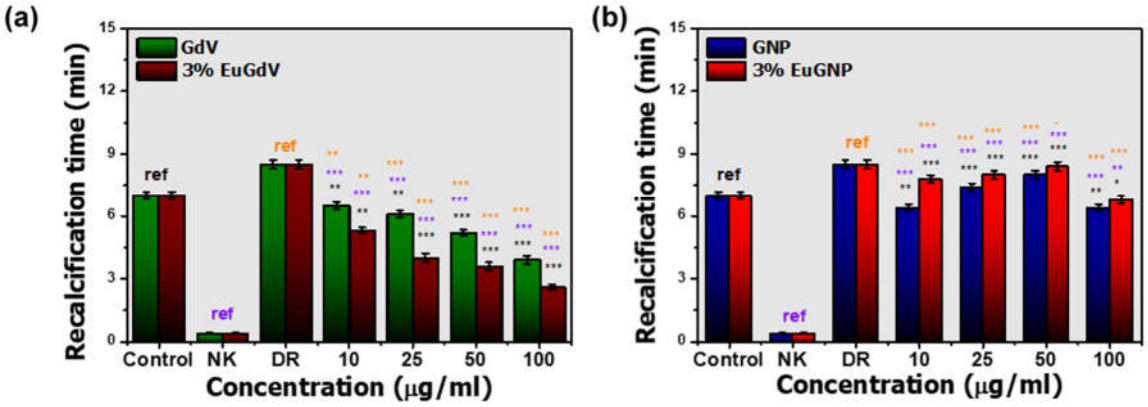

FIGURE 7.9: Comparative plot for plasma recalcification time for various concentrations of (a) GNP, 3% EuGNP (b) GdV and 3% EuGdV respectively. The significant figures are labelled wherein, the symbols imply obtained p-values (* for p< 0.05, ** for 0.001<p<0.01 and *** for 0.001<p).

procoagulant state is associated with the development of thrombosis and is also related to cancer progression as an indicator of poor prognosis [66, 67]. The NPs can in fact modulate coagulation inappropiately and cause pathological thrombosis and hemorrhage, as undesirable side effects [67]. From our observation, GNP and 3% EuGNP nanosystem can be considered compatible to human blood plasma with minimum alteration to coagulation or clotting time. However, the surprising dose dependent delayed coagulation respose of GdV and 3% EuGdV nanosystem can be evaluated as promising anti-coagulation It is known that complete human blood plasma consists of over 3700 different types of proteins, of which several proteins mediate attractive interaction between membranes [68]. Numerous reports demonstrate binding of plasma proteins to NPs surfaces [38, 68-70]. Specifically, most nanosystems interact with biological matrices to be spontaneously coated by plasma proteins, thereby leading to a protein "corona" around the nanoparticle [38]. As a nanomaterial counters a biophysiological environment, it is primarily surrounded by high concentrations of free protein which tend to migrate to the NP surface following diffusion, and/or aided by potential energy gradient [71]. Considering thermodynamically

favorable conditions in the surface, protein adsorption can occur spontaneously in either a single and/or multiple 'domains' i.e. portions of the NP surface that interacts with the protein to be adsorbed agents [71].

Protein coronas are complex and interact differently for different nanosystems [1, 6, 70]. Amongst the several protein types, fibrinogen and immunoglobins are the most abundant and the dynamic corona with human serum albumin and fibrinogen might dominate the particle surface for short periods of time [38]. NP corona can be discussed into two parts: hard corona and soft corona wherein the soft corona interacts primarily with the ambient solution while the hard corona stays bonded to the NP for a relatively longer time which is known as Vroman Effect (VE) [16]. Hard corona, essentially consists of tightly bound proteins of high affinity while soft corona comprises low affinity proteins which can easily be desorbed [71]. In the primary phase of VE, spontaneous adsorption of hard corona proteins (HSA, *Ig*G, and fibrinogen) occurs which, in later phases, can be replaced by soft corona proteins (apolipoproteins and coagulation factors) [71].

In order to determine the possible protein corona formation in our nanostructures, we evaluated their hydrodynamic size in human blood plasma, as demonstrated in **FIGURE 7.10**. Thickness of plasma protein corona (PPC) has a hydrodynamic diameters in the range of 3–15 nm and reportedly provides an additional hydrodynamic diameter of 20–40 nm once adsorbed in form of multiple layers over NP surface [71-73]. Also, the 3% EuGNP nanosystem displayed an increase in hydrodynamic diameter by ~19 nm, suggesting a few layers in the PPC. However, for 3% EuGdV nanosystem, the hydrodynamic size was found to increase by ~77nm implying numerous layers of PPC being adsorbed over the surface. The PPC can contribute to NP aggregation processes thereby increasing the size beyond 200 nm as observed in or case for 3% EuGdV nanosystem (**FIGURE 7.10**) [71].

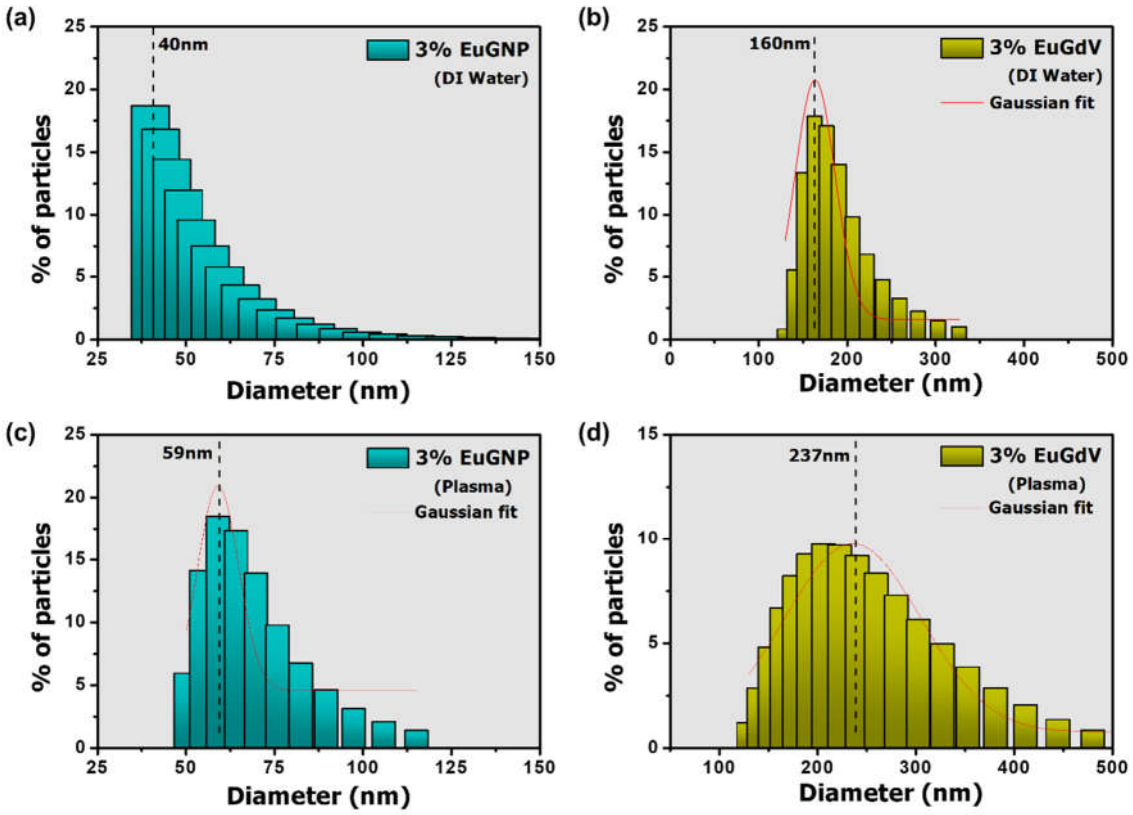

FIGURE 7.10. Hydrodynamic diameter of 3% EuGNP and 3% EuGdV in water is shown in (a, b) respectively; while (c, d) displays the diameter in human blood plasma medium.

It is to be mentioned that in addition to variation in hydrodynamic size of the NPs, the PPC provides a definite value of zeta potential in between ~ 10 - 20 mV nanomaterial, regardless of disparity in NP surface charge (anionic or cationic) or size [71-74]. However, NP surface adsorption of negatively charged plasma/serum proteins results in increased zeta- potential irrespective of the NP surface chemistry [72, 73]. As for negatively charged GdV and 3% EuGdV NPs, increment in entropy upon protein adsorption is not prominent and thereby electrostatic and H-bonding effect supplement the van der Waals interactions [73]. This leads to formation of the highly irreversible PPC in a collective manner instead of being a property of the isolated proteins alone [73]. Adsorption of cationic proteins are facilitated by sequential model of protein binding wherein, proteins bind the colloid, led by binding of anionic proteins to the cationic protein coat [72].

The increased size of the protein-bound particles can affect uptake rate as well as clearance routes [72, 75]. Fibrinogen, a critical component of the blood clotting cascade, constitutes a major portion of protein corona along with other species such as albumin, apolipoproteins, immunoglobulins [72, 73]. Our observations suggest that the GdV based nanosystem upon interaction with human blood plasma, gets covered with several layers of PPC. Such PPC can be constituted of both hard and soft corona proteins viz. fibrinogen and other important coagulation factors which play a decisively dominating role in initiating the coagulation cascade. Due to high affinity, these proteins vital for fibrin formation, are not desorbed from the surface easily and hence inactivation of the enzyme amplifier process is delayed thereby increasing the PRT.

7.3. Conclusion

A dependable approximation of erythrocyte deformability and processes involved are requisite for evaluation of optimal diagnostic as well as therapeutic approaches [76]. It is important to note that, for implementation in biomedical domain of research, RE vanadate nanoparticles are usually functionalized/coated with relevant necessary organic groups that are deemed to reduce their toxicity and high biocompatibility [77]. Moreover, a careful design and fabrication with appropriate functional groups provide other advantages such as- higher thermal stability, enhanced water solubility, increased optical response, higher luminescence intensity and longer decay times [78, 79]. It has been shown also that upconversion emission properties can be tuned upon surface coating due to surface related effects [78]. However, several reports are available that suggest prospective of utilization of bare Eu^{3+} doped RE vanadate nanosystem (without functionalization) in biophysical research areas [47, 80-83]. In this study, bare Eu3+ doped nanosystem were evaluated for their biocompatibility to avoid the complexities involved in surface functionalization. Furthermore, increment in their bio-viability can be protracted in future studies.

The oxide based nanosytem displayed relatively greater hemolytic activity as compared to vanadate based nanosystem which was found to be extremely hemocompatible at concentration as high as 100 μg/ml. Nevertheless, the oxide based NPs can be administered at lower concentrations of 10-25 μg/ml. SEM imaging of RBCs demonstrate the transformations in cell shapes upon treatment with nanostructures. RBCs at various stages of transformation were evident from the images. Interestingly, oxide based NPs displayed minimum alteration in PRT while vanadate based nanostructures were determined to be pro-coagulant at higher concentrations. The effect of hydrodynamic size disparity in human blood plasma has been elucidated with phenomenon of formation of PPC to be considered as prime reason behind the observations. Our observations provide a viable reference for developing effective and biocompatible NPs for nanomedicinal implications.

Bibliography

[1] Türkez, H. and Geyikoğlu, F., An in vitro blood culture for evaluating the genotoxicity of titanium dioxide: the responses of antioxidant enzymes. *Toxicology and Industrial Health*, 23(1):19-23, 2007.

[2] Kang, S.J., Kim, B.M., Lee, Y.J., and Chung, H.W., Titanium dioxide nanoparticles trigger p53-mediated damage response in peripheral blood lymphocytes. *Environmental and Molecular Mutagenesis*, 49(5):399-405, 2008.

[3] Donaldson, K., Stone, V., Seaton, A., and MacNee, W., Ambient particle inhalation and the cardiovascular system: potential mechanisms. *Environmental Health Perspectives*, 109(suppl 4):523-527, 2001.

[4] Liu, T., Bai, R., Zhou, H., Wang, R., Liu, J., Zhao, Y., and Chen, C., The effect of size and surface ligands of iron oxide nanoparticles on blood compatibility. *RSC Advances*, 10(13):7559-7569, 2020.

[5] Aisaka, Y., Kawaguchi, R., Watanabe, S., Ikeda, M., and Igisu, H., Hemolysis caused by titanium dioxide particles. *Inhalation Toxicology*, 20(9):891-893, 2008.

[6] Šimundić, M., Drašler, B., Šuštar, V., Zupanc, J., Štukelj, R., Makovec, D., Erdogmus, D., Hägerstrand, H., Drobne, D., and Kralj-Iglič, V., Effect of engineered TiO_2 and ZnO nanoparticles on erythrocytes, platelet-rich plasma and giant unilamelar phospholipid vesicles. *BMC Veterinary Research*, 9(1):1-13, 2013.

[7] Sharifi, S., Behzadi, S., Laurent, S., Forrest, M.L., Stroeve, P., and Mahmoudi, M., Toxicity of nanomaterials. *Chemical Society Reviews*, 41(6):2323-2343, 2012.

[8] Grzyb, T., Mrówczyńska, L., Szczeszak, A., Śniadecki, Z., Runowski, M., Idzikowski, B., and Lis, S., Synthesis, characterization, and cytotoxicity in human erythrocytes of multifunctional, magnetic, and luminescent nanocrystalline rare earth fluorides. *Journal of Nanoparticle Research*, 17(10):1-18, 2015.

[9] Jasiewicz, B., Mrówczyńska, L., and Malczewska-Jaskóła, K., Synthesis and haemolytic activity of novel salts made of nicotine alkaloids and bile acids. *Bioorganic & Medicinal Chemistry Letters*, 24(4):1104-1107, 2014.

[10] Mrówczyńska, L. and Hägerstrand, H., Platelet-activating factor interaction with the human erythrocyte membrane. *Journal Of Biochemical And Molecular Toxicology*, 23(5):345-348, 2009.

[11] Mukhopadhyay, R., Lim, H.G., and Wortis, M., Echinocyte shapes: bending, stretching, and shear determine spicule shape and spacing. *Biophysical Journal*, 82(4):1756-1772, 2002.

[12] Suwalsky, M., Villena, F., Norris, B., Soto, M., Sotomayor, C., Messori, L., and Zatta, P., Structural effects of titanium citrate on the human erythrocyte membrane. *Journal Of Inorganic Biochemistry*, 99(3):764-770, 2005.

[13] Diez-Silva, M., Dao, M., Han, J., Lim, C.-T., and Suresh, S., Shape and biomechanical characteristics of human red blood cells in health and disease. *MRS Bulletin*, 35(5):382-388, 2010.

[14] Steck, T.L., Red cell shape, in Cell shape: determinants, regulation and regulatory role. Academic Press, New York, 205-246, 1989.

[15] Shah, S.M.T., Yousafzai, Y.M., and Baseer, N., Time dependent changes in red blood cells during storage in the local blood banks of Khyber Pakhtunkhwa. *Journal of the Pakistan Medical Association*:1-16, 2020.

[16] Hao, F., Liu, Q.S., Chen, X., Zhao, X., Zhou, Q., Liao, C., and Jiang, G., Exploring the heterogeneity of nanoparticles in their interactions with plasma coagulation factor XII. *ACS Nano*, 13(2):1990-2003, 2019.

[17] Suntravat, M., Nuchprayoon, I., and Pérez, J.C., Comparative study of anticoagulant and procoagulant properties of 28 snake venoms from families Elapidae, Viperidae, and purified Russell's viper venom-factor X activator (RVV-X). *Toxicon*, 56(4):544-553, 2010.

[18] Quick, A.J., A study of the coagulation defect in hemophilia and in jaundice. *American Journal of the Medical Sciences*, 190:501-511, 1935.

[19] Laloy, J., Minet, V., Alpan, L., Mullier, F., Beken, S., Toussaint, O., Lucas, S., and Dogné, J.-M., Impact of silver nanoparticles on haemolysis, platelet function and coagulation. *Nanobiomedicine*, 1(Godište 2014):1-4, 2014.

[20] Pan, Y., Yang, J., Fang, Y., Zheng, J., Song, R., and Yi, C., One-pot synthesis of gadolinium-doped carbon quantum dots for high-performance multimodal bioimaging. *Journal of Materials Chemistry B*, 5(1):92-101, 2017.

[21] Mortezazadeh, T., Gholibegloo, E., Alam, N.R., Dehghani, S., Haghgoo, S., Ghanaati, H., and Khoobi, M., Gadolinium (III) oxide nanoparticles coated with folic acid-functionalized poly (β-cyclodextrin-co-pentetic acid) as a biocompatible targeted nano-contrast agent for cancer diagnostic: in vitro and in vivo studies. *Magnetic Resonance Materials in Physics, Biology and Medicine*, 32:487-500, 2019.

[22] Siega, P., Wuerges, J., Arena, F., Gianolio, E., Fedosov, S.N., Dreos, R., Geremia, S., Aime, S., and Randaccio, L., Release of toxic Gd^{3+} ions to tumour cells by vitamin B12 bioconjugates. *Chemistry–A European Journal*, 15(32):7980-7989, 2009.

[23] Clutton, S., The importance of oxidative stress in apoptosis. *British Medical Bulletin*, 53(3):662-668, 1997.

[24] Takenaka, S., Karg, E., Roth, C., Schulz, H., Ziesenis, A., Heinzmann, U., Schramel, P., and Heyder, J., Pulmonary and systemic distribution of inhaled ultrafine silver particles in rats. *Environmental Health Perspectives*, 109(suppl 4):547-551, 2001.

[25] Bull, B.S. and Brailsford, J.D., The biconcavity of the red cell: an analysis of several hypotheses. *Blood*, 41(6):833-844, 1973.

[26] Muñoz, S., Sebastián, J., Sancho, M., and Álvarez, G., Elastic energy of the discocyte–stomatocyte transformation. *Biochimica et Biophysica Acta (BBA)-Biomembranes*, 1838(3):950-956, 2014.

[27] Canham, P. and Burton, A.C., Distribution of size and shape in populations of normal human red cells. *Circulation research*, 22(3):405-422, 1968.

[28] Rand, R. and Burton, A., Area and volume changes in hemolysis of single erythrocytes. *Journal of Cellular and Comparative Physiology*, 61(3):245-253, 1963.

[29] Simon, T.L., McCullough, J., Snyder, E.L., Solheim, B.G., and Strauss, R.G. Rossi's principles of transfusion medicine. John Wiley & Sons, 2016.

[30] Rudenko, S.V., Erythrocyte morphological states, phases, transitions and trajectories. *Biochimica et Biophysica Acta (BBA)-Biomembranes*, 1798(9):1767-1778, 2010.

[31] HW, G.L., Wortis, M., and Mukhopadhyay, R., Stomatocyte–discocyte–echinocyte sequence of the human red blood cell: Evidence for the bilayer–couple hypothesis from membrane mechanics. *Proceedings of the National Academy of Sciences*, 99(26):16766-16769, 2002.

[32] Sheetz, M.P. and Singer, S., Biological membranes as bilayer couples. A molecular mechanism of drug-erythrocyte interactions. *Proceedings of the National Academy of Sciences*, 71(11):4457-4461, 1974.

[33] Bratosin, D., Tissier, J.P., Lapillonne, H., Hermine, O., de Villemeur, T.B., Cotoraci, C., Montreuil, J., and Mignot, C., A cytometric study of the red blood cells in Gaucher disease reveals their abnormal shape that may be involved in

increased erythrophagocytosis. *Cytometry Part B: Clinical Cytometry*, 80(1):28-37, 2011.

[34] Jaworski, S., Hinzmann, M., Sawosz, E., Grodzik, M., Kutwin, M., Wierzbicki, M., Strojny, B., Vadalasetty, K.P., Lipińska, L., and Chwalibog, A., Interaction of different forms of graphene with chicken embryo red blood cells. *Environmental Science and Pollution Research*, 24(27):21671-21679, 2017.

[35] Wintrobe, M.M. Wintrobe's clinical hematology. Lippincott Williams & Wilkins, 2008.

[36] Drašler, B., Drobne, D., Novak, S., Valant, J., Boljte, S., Otrin, L., Rappolt, M., Sartori, B., Iglič, A., and Kralj-Iglič, V., Effects of magnetic cobalt ferrite nanoparticles on biological and artificial lipid membranes. *International Journal of Nanomedicine*, 9:1559, 2014.

[37] He, Z., Liu, J., and Du, L., The unexpected effect of PEGylated gold nanoparticles on the primary function of erythrocytes. *Nanoscale*, 6(15):9017-9024, 2014.

[38] Cedervall, T., Lynch, I., Lindman, S., Berggård, T., Thulin, E., Nilsson, H., Dawson, K.A., and Linse, S., Understanding the nanoparticle–protein corona using methods to quantify exchange rates and affinities of proteins for nanoparticles. *Proceedings of the National Academy of Sciences*, 104(7):2050-2055, 2007.

[39] Tian, Y., Tian, Z., Dong, Y., Wang, X., and Zhan, L., Current advances in nanomaterials affecting morphology, structure, and function of erythrocytes. R*SC Advances*, 11(12):6958-6971, 2021.

[40] Strijkova-Kenderova, V., Todinova, S., Andreeva, T., Bogdanova, D., Langari, A., Danailova, A., Krumova, S., Zlatareva, E., Kalaydzhiev, N., and Milanov, I., Morphometry and stiffness of red blood cells—signatures of neurodegenerative diseases and aging. *International Journal Of Molecular Sciences,* 23(1):227, 2021.

[41] Thomassen, L.C., Rabolli, V., Masschaele, K., Alberto, G., Tomatis, M., Ghiazza, M., Turci, F., Breynaert, E., Martra, G., and Kirschhock, C.E., Model

system to study the influence of aggregation on the hemolytic potential of silica nanoparticles. *Chemical Research in Toxicology*, 24(11):1869-1875, 2011.

[42] ZDREMȚAN, D., Calu, L., Mihali, C.V., TUŞA, I.M., Dumitrache, F., Cotoraci, C.A., and Bratosin, D., Characterization of human erythrocytes as carriers for iron nanoparticles. 2020.

[43] Honary, S. and Zahir, F., Effect of zeta potential on the properties of nano-drug delivery systems-a review (Part 1). *Tropical Journal of Pharmaceutical Research*, 12(2):255-264, 2013.

[44] Patil, S., Sandberg, A., Heckert, E., Self, W., and Seal, S., Protein adsorption and cellular uptake of cerium oxide nanoparticles as a function of zeta potential. *Biomaterials*, 28(31):4600-4607, 2007.

[45] Kozelskaya, A., Panin, A., Khlusov, I., Mokrushnikov, P., Zaitsev, B., Kuzmenko, D., and Vasyukov, G.Y., Morphological changes of the red blood cells treated with metal oxide nanoparticles. *Toxicology in Vitro*, 37:34-40, 2016.

[46] Sheetz, M.P. and Singer, S., Equilibrium and kinetic effects of drugs on the shapes of human erythrocytes. *The Journal of Cell Biology*, 70(1):247-251, 1976.

[47] Kim, H., Jeong, H., and Byeon, S.-H., Selective filter effect induced by Cu2+ adsorption on the fluorescence of a $GdVO_4$:Eu nanoprobe. *ACS Applied Materials & interfaces*, 8(24):15497-15505, 2016.

[48] Hu, H., Li, D., Liu, S., Wang, M., Moats, R., Conti, P.S., and Li, Z., Integrin α2β1 targeted $GdVO_4$:Eu ultrathin nanosheet for multimodal PET/MR imaging. *Biomaterials*, 35(30):8649-8658, 2014.

[49] Kang, X., Yang, D., Ma, P.a., Dai, Y., Shang, M., Geng, D., Cheng, Z., and Lin, J., Fabrication of hollow and porous structured $GdVO_4$:Dy^{3+} nanospheres as anticancer drug carrier and MRI contrast agent. *Langmuir*, 29(4):1286-1294, 2013.

[50] Wangkhem, R., Yaba, T., Singh, N.S., and Ningthoujam, R., Surface functionalized $GdVO_4$:Eu^{3+} nanocrystals as turn-off luminescent probe for selective sensing of Cu2+ ions: role of pH. *Applied Surface Science*, 563:150350, 2021.

[51] Ahrén, M., Selegård, L., Söderlind, F., Linares, M., Kauczor, J., Norman, P., Käll, P.-O., and Uvdal, K., A simple polyol-free synthesis route to Gd_2O_3 nanoparticles for MRI applications: an experimental and theoretical study. *Journal of Nanoparticle Research*, 14(8):1-17, 2012.

[52] Aldalbahi, A., Rahaman, M., and Ansari, A.A., Mesoporous silica modified luminescent Gd_2O_3:Eu nanoparticles: physicochemical and luminescence properties. *Journal of Sol-Gel Science and Technology*, 89(3):785-795, 2019.

[53] Ansari, A.A., Ahmad, N., and Labis, J.P., Highly colloidal luminescent porous Tb-doped gadolinium oxide nanoparticles: Photophysical and luminescent properties. *Journal of Photochemistry and Photobiology A: Chemistry*, 371:10-16, 2019.

[54] Zhou, C., Wu, H., Huang, C., Wang, M., and Jia, N., Facile Synthesis of Single-Phase Mesoporous Gd_2O_3:Eu Nanorods and Their Application for Drug Delivery and Multimodal Imaging. *Particle & Particle Systems Characterization*, 31(6):675-684, 2014.

[55] Jain, A., Hirata, G., Farías, M., and Castillón, F., Synthesis and characterization of (3-Aminopropyl) trimethoxy-silane (APTMS) functionalized Gd_2O_3:Eu^{3+} red phosphor with enhanced quantum yield. *Nanotechnology*, 27(6):065601, 2015.

[56] Nel, A., Mädler, L., Velegol, D., Xia, T., and Hoek, E., V; Somasundaran P.; Klaessig F.; Castranova V.; Thompson M. Understanding biophysicochemical interactions at the nano-bio interface. *Nat. Mater*, 8:543-557, 2009.

[57] Kim, M.J. and Shin, S., Toxic effects of silver nanoparticles and nanowires on erythrocyte rheology. *Food and chemical toxicology*, 67:80-86, 2014.

[58] Clark, M.R., Mohandas, N., Feo, C., Jacobs, M.S., and Shohet, S.B., Separate mechanisms of deformability loss in ATP-depleted and Ca-loaded erythrocytes. *The Journal of Clinical Investigation*, 67(2):531-539, 1981.

[59] Li, S.-Q., Zhu, R.-R., Zhu, H., Xue, M., Sun, X.-Y., Yao, S.-D., and Wang, S.-L., Nanotoxicity of TiO_2 nanoparticles to erythrocyte in vitro. *Food and Chemical Toxicology*, 46(12):3626-3631, 2008.

[60] Laloy, J., Minet, V., Alpan, L., Mullier, F., Beken, S., Toussaint, O., Lucas, S., and Dogné, J.-M., Impact of silver nanoparticles on haemolysis, platelet function and coagulation. *Nanobiomedicine*, 1:4, 2014.

[61] Vogler, E.A. and Siedlecki, C.A., Contact activation of blood-plasma coagulation. *Biomaterials*, 30(10):1857-1869, 2009.

[62] Potter, T.M., Rodriguez, J.C., Neun, B.W., Ilinskaya, A.N., Cedrone, E., and Dobrovolskaia, M.A., In vitro assessment of nanoparticle effects on blood coagulation, in Characterization of nanoparticles intended for drug delivery. Springer, 103-124, 2018.

[63] Smith, S.A., The cell-based model of coagulation. *Journal of veterinary emergency and critical care*, 19(1):3-10, 2009.

[64] Laloy, J., Robert, S., Marbehant, C., Mullier, F., Mejia, J., Piret, J.-P., Lucas, S., Chatelain, B., Dogné, J.-M., and Toussaint, O., Validation of the calibrated thrombin generation test (cTGT) as the reference assay to evaluate the procoagulant activity of nanomaterials. *Nanotoxicology*, 6(2):213-232, 2012.

[65] Li, D., Chen, H., McClung, W.G., and Brash, J.L., Lysine-PEG-modified polyurethane as a fibrinolytic surface: effect of PEG chain length on protein interactions, platelet interactions and clot lysis. *Acta Biomaterialia*, 5(6):1864-1871, 2009.

[66] Prandoni, P., Falanga, A., and Piccioli, A., Cancer, thrombosis and heparin-induced thrombocytopenia. *Thrombosis Research*, 120:S137-S140, 2007.

[67] Ilinskaya, A.N. and Dobrovolskaia, M.A., Nanoparticles and the blood coagulation system. Handbook of Immunological Properties of Engineered *Nanomaterials: Volume 2: Haematocompatibility of Engineered Nanomaterials*:261-302, 2016.

[68] Aggarwal, P., Hall, J.B., McLeland, C.B., Dobrovolskaia, M.A., and McNeil, S.E., Nanoparticle interaction with plasma proteins as it relates to particle biodistribution, biocompatibility and therapeutic efficacy. *Advanced Drug Delivery Reviews*, 61(6):428-437, 2009.

[69] Nel, A.E., Mädler, L., Velegol, D., Xia, T., Hoek, E., Somasundaran, P., Klaessig, F., Castranova, V., and Thompson, M., Understanding biophysicochemical interactions at the nano–bio interface. *Nature Materials*, 8(7):543-557, 2009.

[70] Ruh, H., Kühl, B., Brenner-Weiss, G., Hopf, C., Diabaté, S., and Weiss, C., Identification of serum proteins bound to industrial nanomaterials. *Toxicology Letters*, 208(1):41-50, 2012.

[71] Walkey, C.D. and Chan, W.C., Understanding and controlling the interaction of nanomaterials with proteins in a physiological environment. *Chemical Society Reviews*, 41(7):2780-2799, 2012.

[72] Dobrovolskaia, M.A., Patri, A.K., Zheng, J., Clogston, J.D., Ayub, N., Aggarwal, P., Neun, B.W., Hall, J.B., and McNeil, S.E., Interaction of colloidal gold nanoparticles with human blood: effects on particle size and analysis of plasma protein binding profiles. *Nanomedicine: Nanotechnology, Biology and Medicine*, 5(2):106-117, 2009.

[73] Monopoli, M.P., Walczyk, D., Campbell, A., Elia, G., Lynch, I., Baldelli Bombelli, F., and Dawson, K.A., Physical− chemical aspects of protein corona: relevance to in vitro and in vivo biological impacts of nanoparticles. *Journal of the American Chemical Society*, 133(8):2525-2534, 2011.

[74] Alkilany, A.M., Nagaria, P.K., Hexel, C.R., Shaw, T.J., Murphy, C.J., and Wyatt, M.D., Cellular uptake and cytotoxicity of gold nanorods: molecular origin of cytotoxicity and surface effects. *Small*, 5(6):701-708, 2009.

[75] Chithrani, B.D., Ghazani, A.A., and Chan, W.C., Determining the size and shape dependence of gold nanoparticle uptake into mammalian cells. *Nano Letters*, 6(4):662-668, 2006.

[76] Huisjes, R., Bogdanova, A., Van Solinge, W.W., Schiffelers, R.M., Kaestner, L., and Van Wijk, R., Squeezing for life–properties of red blood cell deformability. *Frontiers in Physiology*, 9:656, 2018.

[77] Dong, K., Ju, E., Liu, J., Han, X., Ren, J., and Qu, X., Ultrasmall biomolecule-anchored hybrid $GdVO_4$ nanophosphors as a metabolizable multimodal bioimaging contrast agent. *Nanoscale*, 6(20):12042-12049, 2014.

[78] Ghosh, P., Oliva, J., Rosa, E.D.l., Haldar, K.K., Solis, D., and Patra, A., Enhancement of upconversion emission of $LaPO_4$:Er@Yb core−shell nanoparticles/nanorods. *The Journal of Physical Chemistry C*, 112(26):9650-9658, 2008.

[79] Wang, Y., Qin, W., Zhang, J., Cao, C., Lü, S., and Ren, X., Photoluminescence of colloidal YVO_4: Eu/SiO_2 core/shell nanocrystals. *Optics Communications*, 282(6):1148-1153, 2009.

[80] Nikitchenko, Y.V., Klochkov, V.K., Kavok, N.S., Karpenko, N.A., Nikitchenko, I.V., Yefimova, S.L., and Bozhkov, A.I., Comparative studies of orthovanadate nanoparticles and metformin on life quality and survival of senile wistar rats. *Biological Trace Element Research*, 200(3):1237-1247, 2022.

[81] Karpenko, N., Korenieva, Y.M., Chystiakova, E.Y., Smolienko, N., Bielkina, I., Seliukova, N.Y., Kustova, S., Boiko, M., Larianovska, Y.B., and Klochkov, V., The influence of the rare-earth metals nanoparticles on the rat's males reprductive function in the descending stage of ontogenesis. *Ukrainian biopharmaceutical journal,* (4 (45)):75-80, 2016.

[82] Talib, A.J., Alkahtani, M., Jiang, L., Alghannam, F., Brick, R., Gomes, C.L., Scully, M.O., Sokolov, A.V., and Hemmer, P.R., Lanthanide ions doped in vanadium oxide for sensitive optical glucose detection. *Optical Materials Express*, 8(11):3277-3287, 2018.

[83] Grzyb, T., Mrówczyńska, L., Szczeszak, A., Śniadecki, Z., Runowski, M., Idzikowski, B., and Lis, S., Synthesis, characterization, and cytotoxicity in human erythrocytes of multifunctional, magnetic, and luminescent nanocrystalline rare earth fluorides. *Journal of Nanoparticle Research*, 17:1-18, 2015.